

Design and Analysis of Microfluidic Cell Counter using Spice Simulation

Sheikh Muhammad Asher Iqbal. Nauman Zafar Butt

Abstract:

Microfluidic cytometers based on coulter principle have recently shown a great potential for point of care biosensors for medical diagnostics. In this study, the design and characterization of coulter based microfluidic cytometer are investigated through electrical circuit simulations considering an equivalent electrical model for the biological cell. We explore the effects related to microelectrode dimensions, microfluidic detection volume, suspension medium, size/shape of the target cells, and, the impedance of the external readout circuit, on the output response of the sensor. We show that the effect of microelectrodes' surface area and the dielectric properties of the suspension medium should be carefully considered when characterizing the output response of the sensor. In particular, the area of the microelectrodes can have a significant effect on cell's electrical opacity (the ratio of cell impedance at high to low frequency) which is commonly used to distinguish between sub-populations of the target cells (e.g. lymphocytes vs. monocytes when counting white blood cells). Moreover, we highlight that the opacity response vs. frequency can significantly vary depending upon whether the absolute cell impedance or the differential output impedance is used in the calculation. These insights may provide valuable guidelines for the design and characterization of coulter based microfluidic sensors.

Keywords:

Electrical Cell Model, Microfluidic Cell Counter, Coulter Principle.

1. Introduction:

The interaction of biological cells with an applied electrical field finds many application in medical science (Michelle Khine 2004). . For example, in the process of electroporation, stimulation of cells at a high electrostatic field is used to create pores in the cell membrane which allow for transferring drugs or DNA into the cell []. Similarly, in dielectrophoresis, forces exerted on the cell due to an applied AC electric field are used to separate cells having different size or shape. This technique finds various medical applications such as separating cancer cells from healthy cells, platelets from the whole blood, and, live cells from dead cells, etc. []. A relatively recent application of the electrical interaction of biological cells is in the area of medical diagnostics where microfluidic cell cytometry based on the Coulter principle [] is used to enumerate biomarkers for a particular disease. Other applications of this technique include purification of liquids by detecting particles of impurities, detecting pollens and drug administering. A typical Coulter based cell cytometer can count or sort cells of various types based on the change in the electrical impedance of a $\sim\mu$ -liter volume of an electrolyte as the cells flow across the embedded microelectrodes. In an immunoassay biochip, two identical counters are typically placed, one at the inlet, and, the other at the outlet of a microfluidic immuno-capture chamber. The capture chamber contains antibodies that are specific to the target biomarkers and are usually coated on 3D micro-pillars to enhance the capture efficiency. A differential counting of the biomarker at the entry and the exit of the chamber is used to enumerate the target biomarker. An on-chip electronic circuit for signal processing and data acquisition can potentially be integrated with the microfluidic biochip for the portable biosensor. The main advantages of these electronic biochips are their high precision, label-free detection, portability, and, compatibility with high throughput chip manufacturing process.

One of the prime application of microfluidic cell cytometry is to detect biological cells which leads to diagnosis of fatal diseases like HIV/AIDS and Cancer. Currently, there are about 36.4 million people globally being affected by HIV/AIDS and their number is increasing at a rate of 5000 new infections per day (HIV.GOV 2017). Around 11 million (30%) of these HIV/AIDS patients did not have access to HIV testing services. Therefore, a microfluidic point of care device could provide a low cost and accessible solution for such epidemics. Immunoassays based on Coulter based microfluidic enumeration of biomarkers in a drop of blood sample have recently attracted a lot of attention for point of care (PoC) medical diagnostics (Watkins 2013; Hassan 2017). A variety of applications have been demonstrated including stratification of sepsis based on the real-time quantification of CD64 and cytokines, and, HIV/AIDS prognostics using CD4 enumeration (Hassan 2017). More recently, PoC microfluidic immunoassays based on Coulter principle have been applied to enumerate proteins in a drop of whole blood (Valera 2018).

Previously, Jian Chen (2015) has summarized developments in cell characterization in a chronological order. Gawad (2001) has demonstrated an impedance spectrometry microfluidic cytometer for cell analysis and sorting where 3D finite element simulation were used to compare different cell geometries. Gawad (2001) has used a simplified version of the electrical model for the biological cell. Premkumar Ellappan (2005) has presented a simulation study on an elaborated electrical model for the cell that was originally introduced by Schoenbach et al (2002). The Cadence Spectra tool was used to study the response of the cell model at variable signal frequency and cell parameters. Furthermore, Xiaolong Qiu (2018) has optimized the microfluidic channel to improve the hydrodynamic dissociation of cells from tissues and organs which leads to cell identification and disease diagnosis. Vibha Jayara (2013) has optimized the microfluidic channel for the cell growth and has described the approaches taken to fabricate, optimize, and validate a biocompatible device. The experimental observations revealed in that study showed that the attempt to increase the channel depth could induce surface roughness, which could significantly affect the device characteristics. Watkins (2013) has developed a differential microfluidic cytometry technique for the CD4⁺ and CD8⁺ lymphocyte counter that were demonstrated for HIV diagnostic applications as an effective indicators for the patient's immune system and HIV infection. Umer Hassan ([nature protocol paper](#)) has published detailed protocols for the fabrication of differential microfluidic cytometer biochip. Umer Hassan (2015) demonstrated the application of the differential microfluidic cell counter biochip for the complete blood cell counts at point of care. Moreover, Umer Hassan (2017) used the differential cell counter biochip to characterize CD 64 cells from the whole blood samples for sepsis stratification. More recently, Valera (2018) has demonstrated another application of differential cell counter microfluidic biochip platform for electrical quantification of proteins in blood samples.

Although a large number of studies have demonstrated the application of microfluidic cytometer for a variety of biomarkers' detection, the design aspects of the cytometer and a systematic analysis of its performance as a function of cellular properties and those of the suspension medium are relatively unexplored in the literature. In particular, a detailed electrical characterization or modeling of the microfluidic cytometer system which could guide the device design and help in the interpretation of experimental data is lacking. In this paper, we use electrical circuit simulations to uncover some of the design insights and guidelines for the optimized structural and circuit parameters of the device. In particular, we have explored the effects of microelectrode dimensions, medium's impedance and its dielectric properties, readout circuit's resistance, and, the dimensions of the microfluidic channel on the electrical output of the sensor. Moreover, we explore the electrical response of the sensor as a function of varying the cell properties such as cytoplasm and nuclear impedances, and, membrane capacitance. Finally, the electrical opacity for the cells which can provide useful information about cell membrane properties is discussed in context of the design parameters and the input signal frequency.

2. Modelling Approach:

The detection of cell biomarker in a microfluidic counter is based on sensing the difference in the impedance inside a detection volume as the cell traverses through it. In the literature, the cell impedance in a suspension medium has been modeled through several approaches (Morgan 2007). These include the finite element/difference methods (Asami 2006), equivalent circuit model (Foster 1989, Gisma 1998), the boundary element method (Sekine 2000), the transport lattice method (Gowrishankar 2003, Stewart 2005). We have used the equivalent circuit model approach in this work. Although this approach is simpler as compared to other

approaches, it can be very useful to highlight the qualitative trends important for the design and characterization of the device.

The equivalent circuit model is implemented in LT Spice (LTspice) which is a high performance SPICE (Simulation Program with Integrated Circuit Emphasis) tool widely used for simulating electrical circuits. The output voltage signal from the microelectrode sensor is monitored as a function of broad range of physical design parameters for the applied electrical signal frequency ranging from 100 Hz to 100 MHz.

2.1. Cell Electrical Model:

Fig.1a shows an illustration of a biological cell that consists of a cell membrane, cytoplasm and nucleus. We use an equivalent electrical model of cell presented in (Schoenbach 2002) as shown in Fig. 1b. The cell has been modelled as a uniform conductive medium, i.e., cytoplasm having a nucleus and an outer cell membrane. The cell membrane has been modelled as a bilayer spherical dielectric having capacitance, C_m ($\frac{\kappa\epsilon A}{d}$). Nucleus of the cell is modelled as a double lipid bilayer having capacitance, C_n , which is half of that of C_m . The cell's cytoplasm is modelled as a resistance, R_c . The combined impedance of the suspension medium (excluding cells) including different reagents that may be present in the microfluidic detection volume is represented by the resistance of solution (R_{sol}). A double layer capacitance, C_{dl} appears at the interface between a conductive electrode and an adjacent liquid electrolyte (Hou, 2014). Following the approach described in (Premkumar, 2005 and K. Schoenbach 2002) we take $R_c = 16.7K\Omega$, $R_{c2} = 133K\Omega$, $R_{c3} = 16.7K\Omega$, $C_m = 4pF$, $C_n = 2pF$ and $R_n = 133K\Omega$ for our reference target cell while perturbation to these reference values are specified when used. The amplitude (\parallel) and phase (\angle) of the cell impedance, (Z_{cell}) as function of frequency (f) of the applied voltage are plotted in Fig. 1c. Since amplitude of a capacitor's impedance scales with $\frac{1}{2\pi f C}$, $|Z_{cell}|$ decreases with increasing f until all of the capacitive elements in Z_{cell} becomes negligibly small (i.e., the capacitors behave like a short circuit). For $f > 100KHz$, the amplitude of Z_{cell} saturates to a minimum value while its phase approaches to zero (a characteristic of a pure resistive circuit).

2.2. Device Structure:

Fig 1d shows an illustration of the microfluidic cell counter. The device contains three coplanar micro electrodes immersed in the microfluidic detection volume. We assume detection volume of $15 \times 15 \times 15 \mu m^3$ for our simulation results unless otherwise specified. An AC electrical voltage signal of 1V amplitude is applied at the middle microelectrode while voltages at the remaining two microelectrodes are detected. The readout circuit comprises of two identical external resistances (R_{out}), which form a Wheatstone bridge connection with the microfluidic impedances (Fig.1e).

2.3. Sensing Principle:

A microfluidic counter based on coulter principle senses the cells or polystyrene beads coated with proteins individually as they flow through the microelectrodes in a microfluidic channel having detection volume close to the diameter of a single target cell (or bead). As a cell traverses through the detection volume, it induces an electrical pulse at the microelectrodes due to a difference in the impedance between the biological cell and that of the background electrolyte medium. This electrical pulse is sensed across R_{out} . A differential voltage (ΔV_{out}) is sensed at the output of the cell counter by taking the difference between V_{out1} (when detection volume contains a cell) and V_{out2} (when there is no cell in detection volume) measured across R_{out1} and R_{out2} respectively:

$$|\Delta V_{out}| = |V_{out1}| - |V_{out2}| = |I_1 Z_{cell} - I_2 R_{sol}| \quad (a)$$

where I_1 and I_2 are the AC currents flowing through Z_{cell} and R_{sol} respectively. In our modeling approach, we calculate V_{out1} assuming that the cell is exactly in the middle of the detection volume. Fig 2a and 2b show an example for the amplitude and phase of V_{out1} and V_{out2} respectively. Since V_{out2} is influenced by C_{dl} and R_{sol} while V_{out1} is influenced by C_{dl} and Z_{cell} , their frequency response is different. In particular, V_{out2} for the given design shows saturation at a lower frequency as compared V_{out1} . Moreover, at high f ($> 1MHz$), $Z_{cell} > R_{sol}$ for this device, so the saturated amplitude for V_{out2} is greater than that of V_{out1} . The resultant characteristics for ΔV_{out} are shown in Fig 2c. Fig. 2

indicates that the design of device parameters (which influence C_{dl} and R_{sol}) and the cell's size/shape characteristics (which influence its capacitances and resistances) both can affect the sensor's output response. It should be noted that the frequency response of the sensor is significant for the cell analysis because the cell morphology (primarily the membrane capacitance) primarily affects ΔV_{out} at a specific range of frequency (typically around $1MHz$). The ratio between the output responses at a higher frequency to that at a lower frequency is therefore often used to extract valuable information about the cell shape and morphology (Watkins 2013; Hassan 2016; Gawad 2001). This aspect is explored in detail in Section 3.

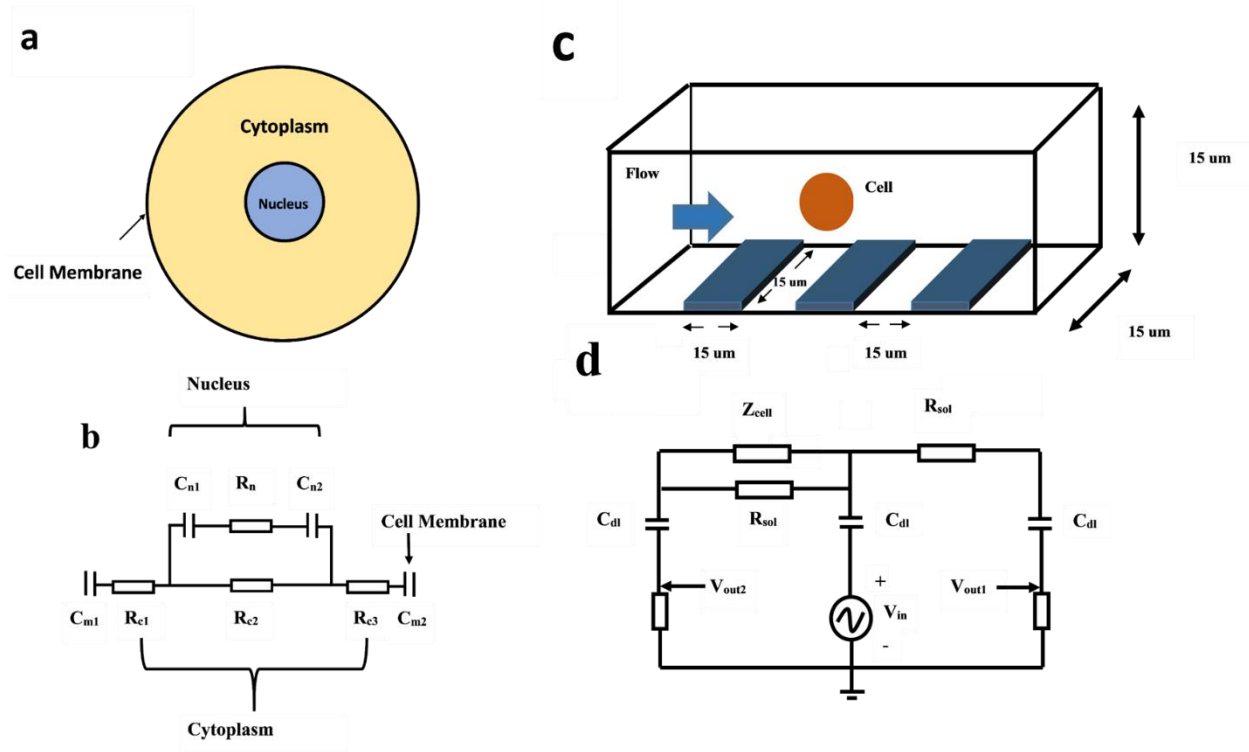


Fig. 1 **a** Illustration of a biological Cell. **b** Circuit Model for cell impedance (Z_{cell}). **c** Illustration of microfluidic cytometer device. **d** Electrical Circuit for the cell counter.

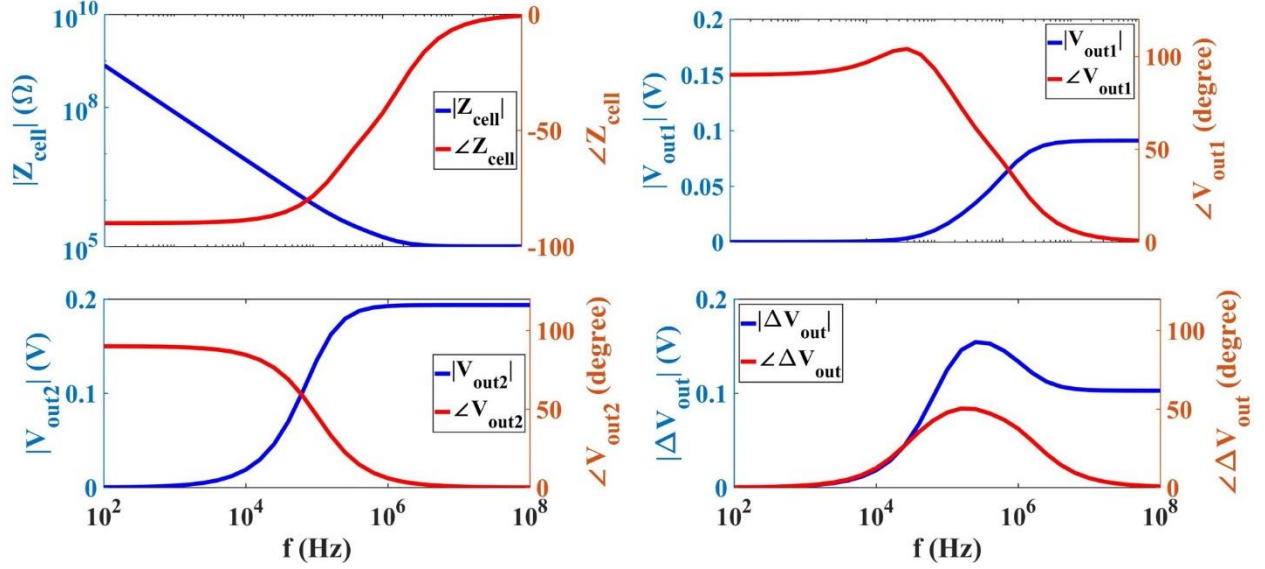


Fig. 2 a impedance of cell (amplitude and phase) b Output voltage at a single microelectrode when cell occupies the detection volume. c Output voltage (amplitude and phase) vs Frequency at a single microelectrode when there is no cell in the detection volume. d Amplitude and Phase of differential voltage ($\Delta V_{out} = V_{out1} - V_{out2}$) vs Frequency of the applied electrical signal.

3. Results and Discussions:

In this section the simulation and design of the microfluidic cytometer device is discussed in detail. The results and discussion are covered into four parts concerning: (i) Device parameters that include microelectrode dimensions and R_{out} , (ii) Suspension medium parameters which includes its dielectric constant and R_{sol} , (iii) Microfluidic channel design parameters which includes the dimensions of the detection volume, and (iv) Cell (biomarker) parameters which include electrical parameters related to its size/shape.

3.1. Device Parameters:

Device parameters include optimizing electrode dimensions and external resistance, R_{out} .

3.1.1. Optimizing Microelectrode Dimensions:

As the surface area (A) of the microelectrodes is directly proportional to C_{dl} , it can influence the output voltage response of the sensor. Fig 3 shows that the amplitude and phase of ΔV_{out} both can indeed be significantly modified with the change in A . As the electrode area increases, the low frequency response of ΔV_{out} is improved. Since the impedance associated with capacitances in the circuit reduces at high f ($> 1MHz$), $|\Delta V_{out}|$ saturates to a maximum value which is determined by R_{sol} and the cell resistances. It can be noted that for an area of $200 \times 200 \mu m^2$, the low frequency response of ΔV_{out} is most broad. For example, at $f = 10 KHz$, ΔV_{out} for $A=200 \times 200 \mu m^2$ and $A=10 \times 10 \mu m^2$ is 0.19 V and 0.7 mV, respectively, hence a shift of about 0.189 V. As f increases to $\sim 1.5 MHz$, $|\Delta V_{out}|$ saturates to a maximum of 0.1 V irrespective of A . Fig. 3c shows $|\Delta V_{out}|$ as function of A for $f = 100KHz$ and $f = 1MHz$ in Fig 3c. While the microelectrode area has negligible effect on $|\Delta V_{out}|$ for $f = 1MHz$, it significantly affects $|\Delta V_{out}|$ for $f = 10kHz$. It should be noted that an optimal value of A which can maximize the low frequency response of the sensor is slightly above $A = 10^4 \mu m^2$. A further increase in A above this optimal value does not provide any additional benefit to the low frequency response of the sensor. Very small values (e.g., $< 10^3 \mu m^2$, on the other hand, significantly degrade the sensor's output response for $f < 100kHz$).

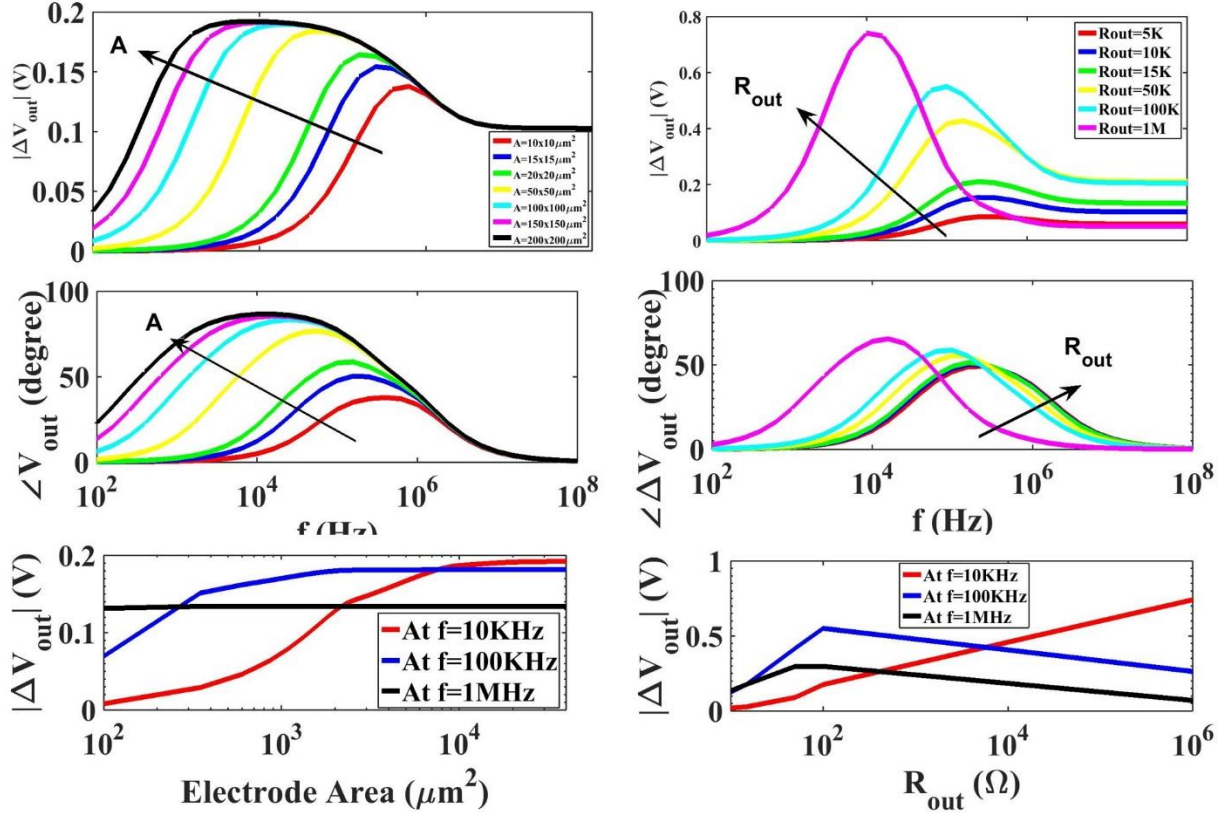


Fig. 3 a $|\Delta V_{out}|$ at varying electrode area. b $\angle \Delta V_{out}$ at varying electrode area. c $|\Delta V_{out}|$ with varying electrode area at two different frequencies. d $|\Delta V_{out}|$ at varying external resistors, R_{out} . e $\angle \Delta V_{out}$ at varying external resistor. f $|\Delta V_{out}|$ at varying external resistors and at two different Frequencies

3.1.2. Optimizing R_{out} :

Fig 3d-f shows ΔV_{out} trends with varying R_{out} . It should be noted that the choice of R_{out} not only influences $|\Delta V_{out}|$ at high frequency but could also affect its low frequency response. As R_{out} is increased above $5\text{K}\Omega$, the $|\Delta V_{out}|$ both at high and low frequencies show an improvement. Increasing R_{out} above 50K however starts to degrade the ΔV_{out} at high frequency but the low frequency response keeps showing an improvement. Fig 4b shows that the choice of R_{out} is dependent on f . At $f = 100\text{KHz}$, an optimal R_{out} is $1\text{M}\Omega$ whereas at higher frequencies i.e. 1MHz optimal R_{out} is $50\text{K}\Omega$. These results highlight that the choice of R_{out} must be made with consideration of the expected range of operating frequency of the cytometer.

3.2. Trends with suspension medium parameters:

The suspension medium parameters include the resistance (R_{sol}) and dielectric constant (κ).

3.2.1. Resistance of the suspension medium:

In a practical implementation of the microfluidic cytometer, the cells are counted directly from a lysed blood sample or blood plasma. Other reagents such as phosphate buffer solution (PBS) and deionized water (DI) etc. can sometimes be incorporated as suspension medium for cells or beads in the laboratory characterization. The value of R_{sol} can be calculated from the conductivity of the solution medium for a given dimension of the detection volume. Fig 5 shows the effect of R_{sol} on ΔV_{out} . It can be seen that highest ΔV_{out} is obtained when PBSx10 is the medium due to its high conductivity 12.3 Sm^{-1} (Lenntech). For a Phosphate Buffered Solution (PBSx1) medium (conductivity of 1.6 Sm^{-1}) and the whole blood sample having conductivity of 1.09 Sm^{-1} (PMC), ΔV_{out} at frequency 1MHz is approximately 80mV and 134mV respectively. For *DI water* solution, conductivity ($5.5 \times 10^{-6} \text{ Sm}^{-1}$ (AmericanBio)), is very low and results in a significant drop in ΔV_{out} .

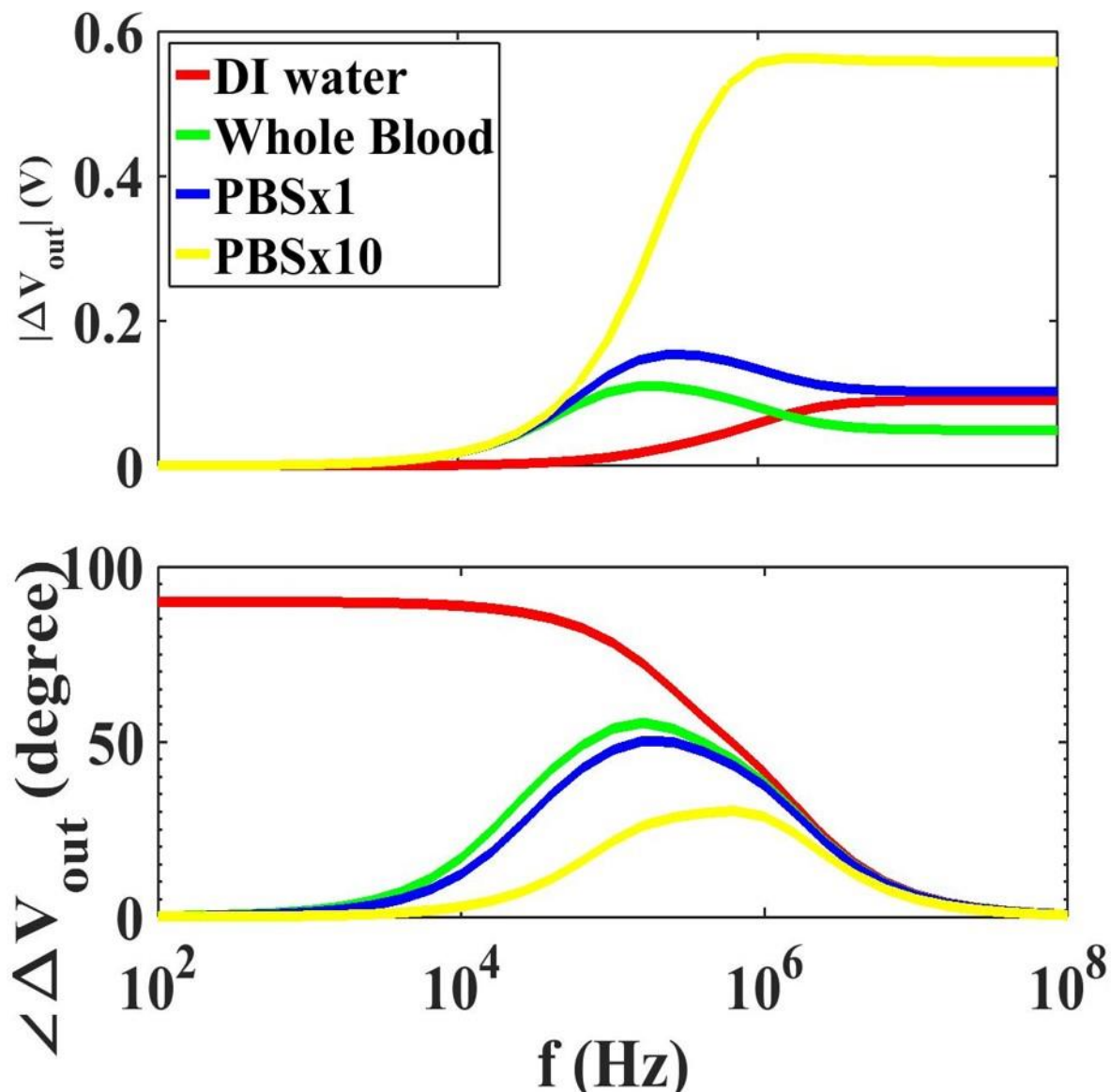


Fig. 4 a $|\Delta V_{out}|$ with different solutions. b $\angle V_{out}$ with different solutions.

3.2.2. Trends with Dielectric constant:

The dielectric properties of the solution medium affect C_{dl} and hence the electrical response of the cytotometer. Fig. 6a shows the plot between the ΔV_{out} and dielectric constants of different electrolyte solutions and $A = 15 \times 15 \mu m^2$.

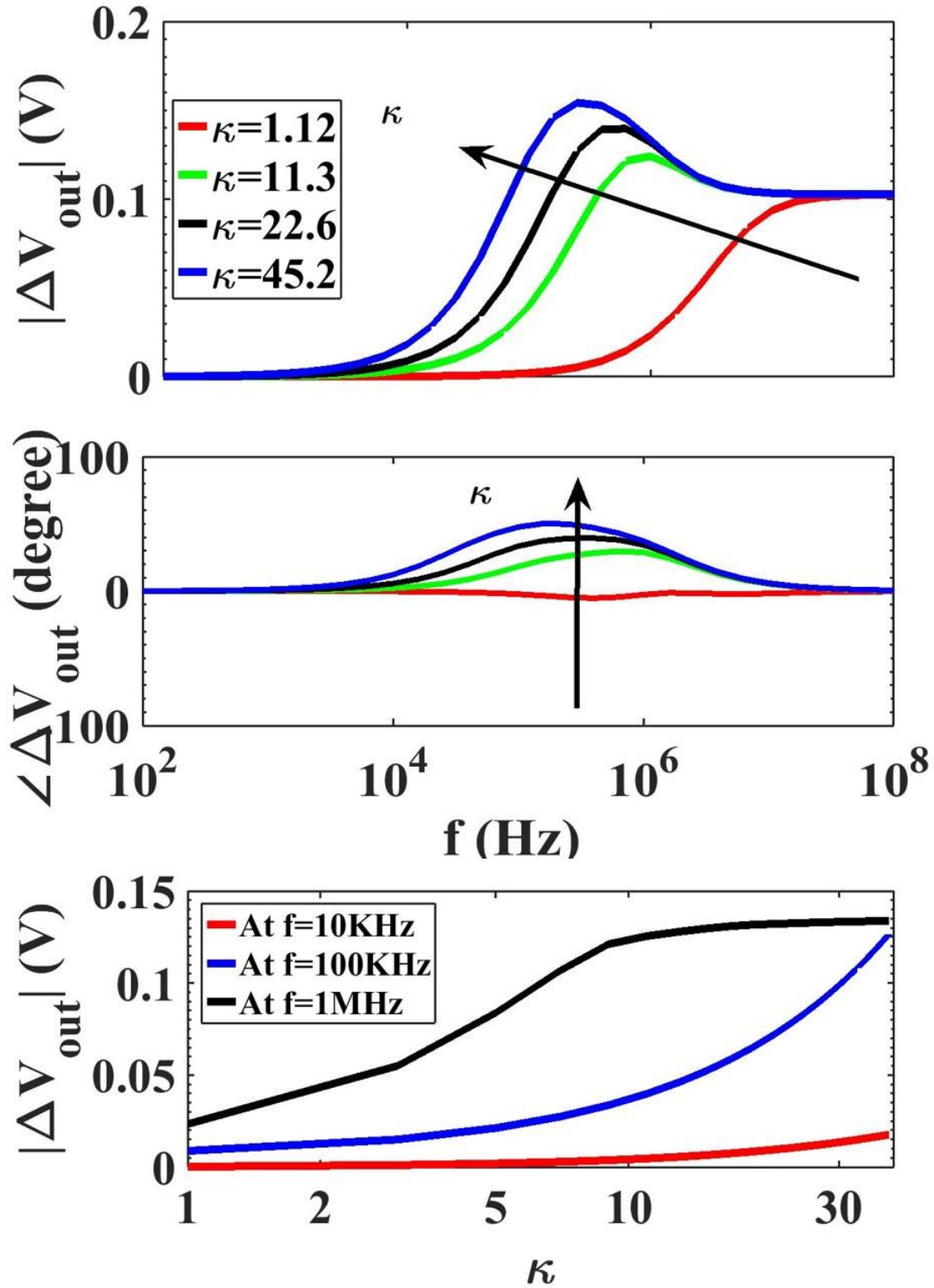


Fig. 5 a $|\Delta V_{out}|$ with varying dielectric constant, κ . b $\angle \Delta V_{out}$ with varying dielectric constant, κ . c $|\Delta V_{out}|$ with varying dielectric constant, κ at two different frequencies.

It can be seen in Fig 6a that the effect of increasing κ improves the low frequency of the cytometer. This trend is similar to what has been shown in Fig. 3a for ΔV_{out} response as a function of A . This is expected since both A and κ affect the C_{dl} similarly at all frequencies of the applied signal. Fig. 6 shows that the effect of κ on ΔV_{out} is more drastic when $\kappa < 10$.

3.3. Trends with Channel Dimensions:

The analysis shown so far has assumed an ideal structure where the cell volume is identical to the detection volume. This is although an ideal situation but in practice may not be possible to implement due to variable cell size distribution of the target cells. Though the qualitative trends for ΔV_{out} are expected to be the same, the structural non-idealities could affect the cytometer's output signal.

In Fig. 7a, $|\Delta V_{out}|$ for a target cell of $15\mu m$ diameter is observed as the detection volumes is varied from $15 \times 15 \times 15 \mu m^3$ (ideal case) to $50 \times 50 \times 50 \mu m^3$. The maximum $|\Delta V_{out}|$ is obtained for the ideal case while a decrease in $|\Delta V_{out}|$ is observed as detection volume is increased. This is expected because a non-ideal detection volume adds additional paths other the cell between the microelectrodes thereby decreasing the electric field intensity across the cell and hence the ΔV_{out} .

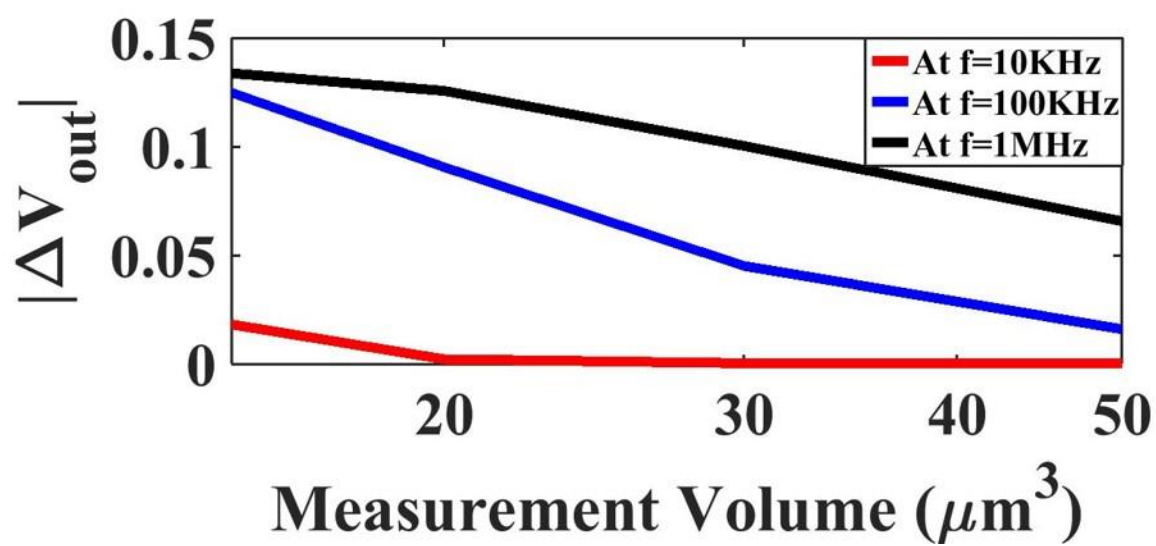
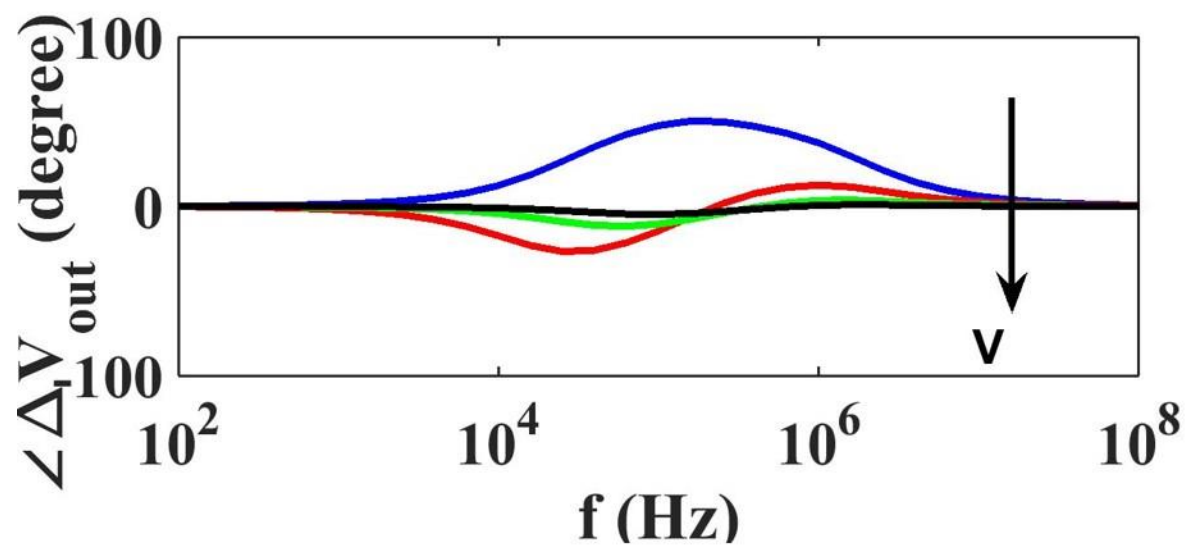
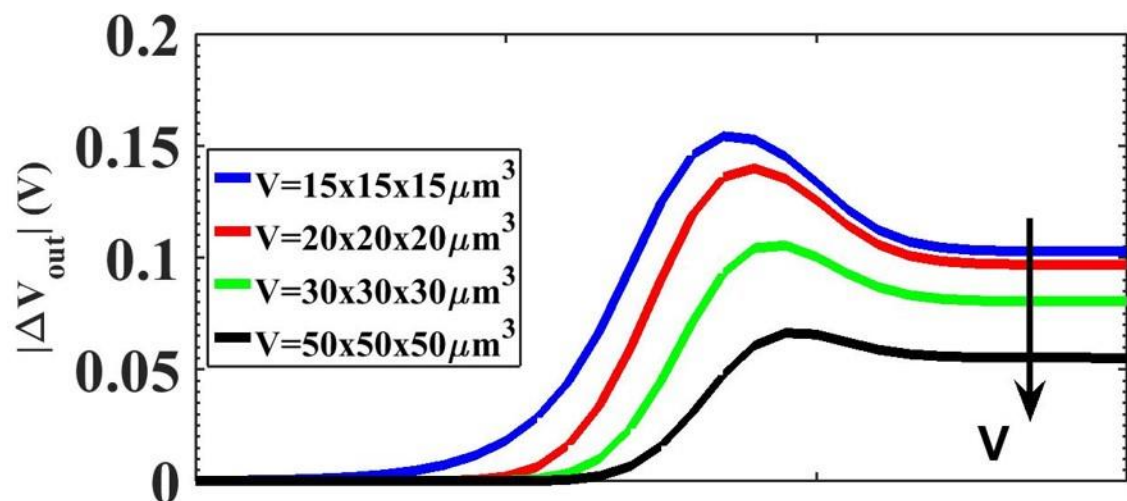


Fig. 6 a $|\Delta V_{out}|$ with varying detection volume exhibiting non idealities¹. **b** $\angle \Delta V_{out}$ with varying detection volume exhibiting non idealities **c** $|\Delta V_{out}|$ at varying detection volume.

3.4. Effect of Cell parameters:

The analysis done so far has been done without varying the cell impedances shown in the cell model (Fig. 1). In practice, however, the cell impedances may vary across a wide range based on the size, type, and, morphology of the cell. For example, for complete blood counting (CBC) test, a microfluidic cytometer needs to simultaneously enumerate Red Blood Cells (RBCs), White Blood Cells (WBCs), and, platelets, etc. (Hassan 2015). Moreover, the sub-populations of lymphocyte, granulocytes, and, monocytes in WBC can be separated out from the counted WBCs. In such experiments, ΔV_{out} and electrical opacity from microfluidic cytometers have often been used to distinguish between various types of blood cells as well as the sub-populations. In Fig 9-13, we show the response of ΔV_{out} and opacity for varying the electrical parameters of the cell. We highlight that the frequency response and amplitude for both ΔV_{out} and opacity are highly dependent on the design of the device, in particular, the surface area of microelectrodes.

3.4.1. Output Voltage (ΔV_{out}) Response:

Fig. 9a and 9b shows the effect of varying cell membrane capacitance, C_m , on amplitude and phase of ΔV_{out} respectively. These results have been plotted for two different surface areas ($A_1 = 15 \times 15 \mu m^2$ and $A_2 = 200 \times 200 \mu m^2$) for the microelectrodes keeping all other cell/device parameters constant. For A_1 , the effect of C_m is significant in range of f between $0.1 MHz - 4 MHz$. For A_2 , however, the effect of varying C_m is significant in a range of $f = 2.5 KHz - 4 MHz$. Fig. 9c shows modulation in cell opacity (defined as $\frac{\Delta V_{out}(LF)}{\Delta V_{out}(HF)}$) where HF is the high frequency which is kept constant at $1 MHz$ and LF is the low frequency which is varied. A significant modulation can be observed in cell opacity for the case of A_1 while for A_2 , the opacity does respond significantly with varying C_m but within a large frequency range. Since opacity is often used to distinguish cell populations on the basis of membrane properties (irrespective of cell size), the results in Fig. 9c highlight some important observations. Firstly, it is evident that there is a specific range of low frequency that provides a significant modulation in opacity. For frequencies which are outside this range, the device response to opacity becomes negligibly weak. Secondly, the optimal range for observing opacity modulation highly varies with the microelectrode dimensions due to the effect of C_{dl} .

3.4.2. Opacity Response:

The electrical opacity (Op) is defined as the ratio of cell impedance at low frequency to that at a higher frequency. This parameter has been shown to respond to the variation in membrane properties independent of the cell size. For microfluidic coulter cytometers, Op is commonly characterized through the response of output voltage at low vs. that at high frequencies. Many studies have used the differential impedance (or equivalently ΔV_{out}) for characterizing Op. We explore Op as a function of variation in cell parameters and show that the Op characterization can be highly dependent on whether the cell impedance or the differential impedance. Fig. shows the

¹ Sol: $PBS \times 1 R_{out} = 15 K \Omega$ $EA = 200 \times 200 \mu m^2$ $C_{dl} = 40 \mu F cm^{-2}$

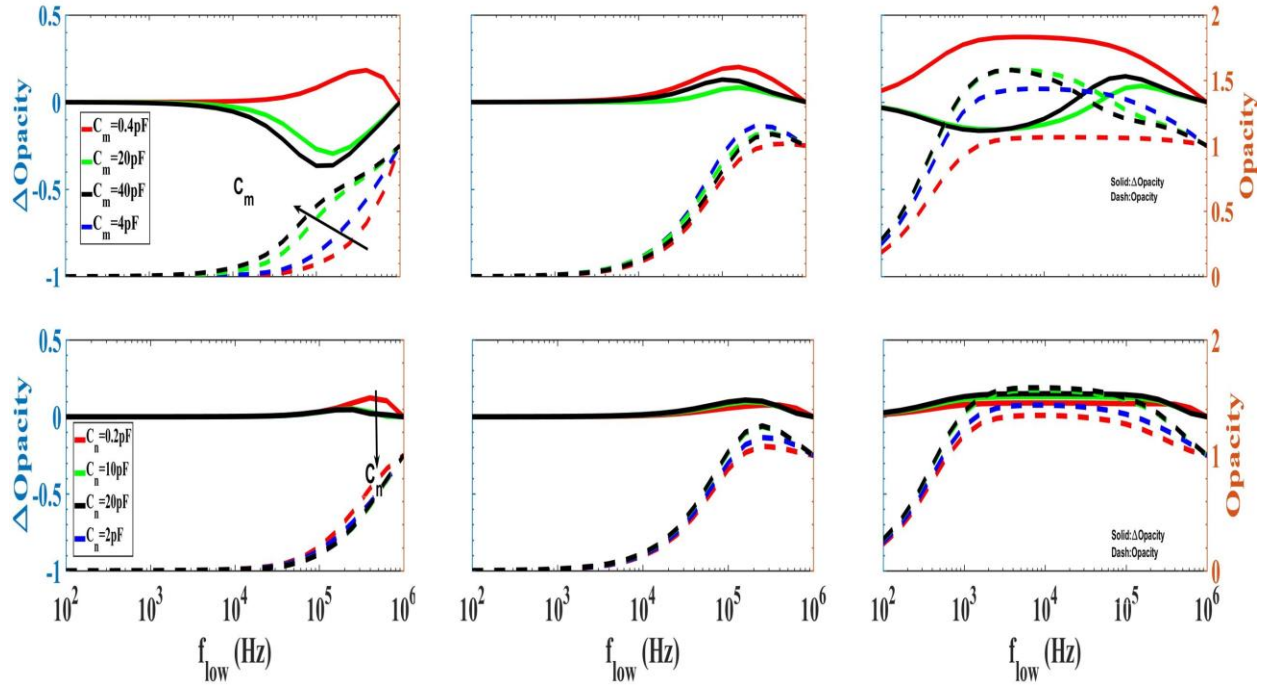


Fig. 7 **a** Opacity Vs frequency evaluated with varying C_m at V_{out1} and A_1 . **b** Δ Opacity evaluated with varying C_m at ΔV_{out} and A_1 . **c** Δ Opacity evaluated with varying C_m at ΔV_{out} and A_2 . **d** Opacity Vs frequency evaluated with varying C_n at V_{out1} and A_1 . **e** Δ Opacity evaluated with varying C_n at ΔV_{out} and A_1 . **f** Δ Opacity evaluated with varying C_n at ΔV_{out} and A_2 .

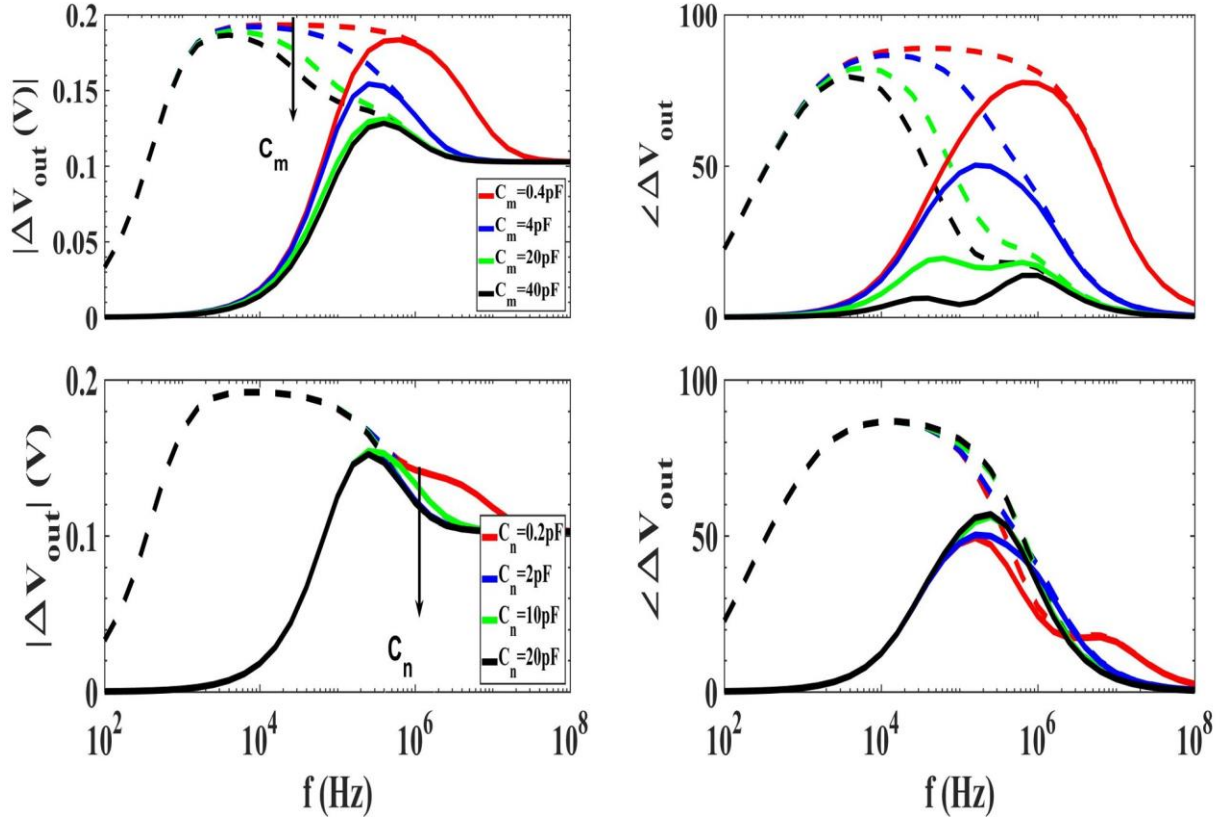


Fig. 8 **a** $|\Delta V_{out}|$ with varying cell membrane, C_m . **b** $\angle \Delta V_{out}$ with varying cell membrane, C_m . **c** $|\Delta V_{out}|$ with varying cell membrane, C_n . **d** $\angle \Delta V_{out}$ with varying cell membrane, C_n .

3.4.3. Trends with varying Cytoplasm Resistance, R_c .

Fig. 10a and 10b shows the ΔV_{out} trends for varying Cytoplasm Resistance, R_c for the two microelectrode area ($A_1 = 15 \times 15 \mu\text{m}^2$ and $A_2 = 200 \times 200 \mu\text{m}^2$). In contrast to the trends for C_m , it can be seen that variation in R_c primarily modulates the amplitude of ΔV_{out} for $f > 100\text{kHz}$ for both A . Fig. 10c and 10d show the effect of R_c on $\Delta\text{Opacity}$ for A_1 and A_2 respectively. It is again evident that the effect of R_c on opacity is quite weaker when $f < 10\text{kHz}$, as compared to that observed for C_m . This is consistent with the fact that opacity is known to be primarily influenced by the membrane properties while R_c is mainly determined by the size of the cell.

3.4.4. Trends with varying Nucleus Capacitance, C_n .

Fig 11a and 11b shows the effect of Nucleus Capacitance, C_n , on ΔV_{out} . In contrast to C_m , the effect of C_n variation on the output voltage is remarkably lower. This is consistent with the electrical cell model in Fig. 1b which illustrates that C_m shares a parallel path to the electrical current with a relatively big membrane resistance and therefore

has a much stronger effect in modulating the voltage across the cell as compared to C_n . Moreover, Fig. 11c highlights that C_n modulation has negligible effect on opacity.

3.4.5. Trends with varying Nucleus Resistance, R_n .

Fig 12a and 12b show the effect of Nucleus Resistance, R_n , over ΔV_{out} which looks quite similar to that observed for R_c in Fig. 10. The effect of R_n on Δ Opacity for A_1 is shown in Fig. 12c. Similar to the trend for R_c , Δ Opacity response to R_n is quite weaker as compared to that observed for C_m in Fig. 9c.

Above results give insight into identification cells based on their type, size, and, membrane properties. As the amplitude of ΔV_{out} at high frequency ($\sim 1MHz$) modulates with R_c and R_n variation, different cells can therefore be identified based on their sizes with impedance measurement at high frequency. Moreover, when membrane properties are the primary difference between sub-populations, modulation in opacity can be an effective way to isolate their counts.

For example, for complete blood cell (*CBC*) count, a whole blood sample containing various white blood cells like lymphocytes and granulocytes/monocytes then Fig 10a and 13a shows that with the decrease in R_c and R_n , ΔV_{out} increases. Amplitude of ΔV_{out} less than 0.6 V corresponds to lymphocytes and above that corresponds to granulocytes/monocytes as lymphocytes have size in between 8 – 12 μm and granulocytes/monocytes have size 12 – 15 μm . This in accordance to what Umer Hassan (2015) had also reported experimentally. Moreover, decrease in R_c and R_n with the size is in accordance with equation (c), as with the increase in size, area of cell increases and hence R_c and R_n decreases (P. Ellappan 2005).

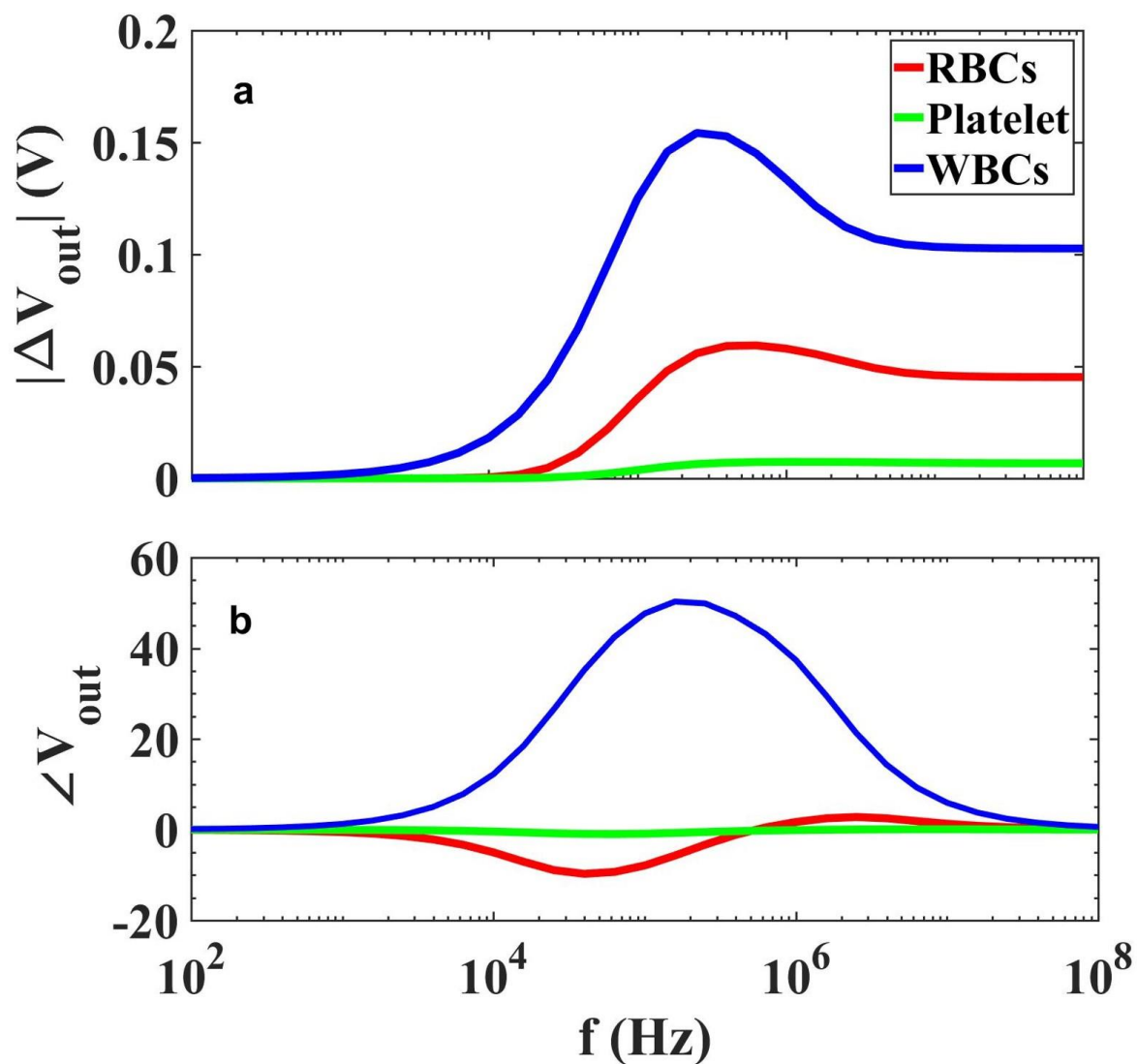


Fig:9 a $|\Delta V_{out}|$ of different cell types b phase of ΔV_{out} of different cell types

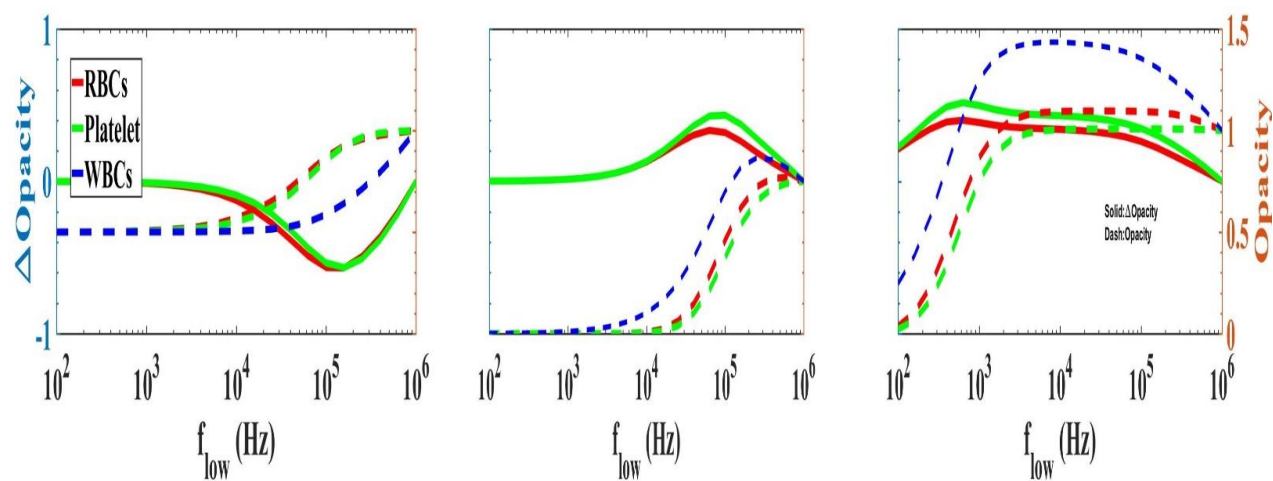


Fig:10 a Opacity Vs frequency evaluated with varying cells at V_{out1} and A_1 . **b** Δ Opacity evaluated with varying cells at ΔV_{out} and A_1 . **c** Δ Opacity evaluated with varying cells at ΔV_{out} and A_2 .

5. Conclusions:

The physical properties of the target biomarker and the structural design of the microfluidic counter have significant effect on the output response of the coulter microfluidic cytometer. We have used circuit simulations based on equivalent cell model to quantify the impact of various device design parameters and the target cell characteristics on the output response of the device. The physical dimensions of the microelectrodes can strongly influence the frequency response of the sensor. The sensor's output signal at lower frequency can be significantly improved with increasing microelectrode surface area. This trend saturates at microelectrode area close to $200 \times 200 \mu\text{m}^2$. The detection volume should optimally be close to the size of the target cell. A detection volume bigger than the target cell size degrades the higher frequency response while lower frequency response is less affected. The dielectric properties of the suspension medium and its electrical impedance can affect the lower and higher frequency response of the counter respectively. The output response does vary with the value of the resistance of the readout bridge circuit. The optimal selection for the readout resistor is dependent on the choice of the signal frequency. The cell's electrical opacity is shown to be strongly vary depending upon whether the absolute cell impedance or the differential output impedance is used in its calculation. The opacity response also requires a careful selection of signal frequencies. With optimally designed device structure, a microfluidic counter can effectively sense the target cells at signal frequency as low as few *KHz*. These insights can provide valuable guidelines for the design and characterization of coulter based microfluidic sensors.

References

1. J. Chen, C. Xue, Y. Zhao, D. Chen, M. Wu and J. Wang, *Int. J. Mol. Sci.* 2015, 16.
2. P. Ellappan, R. Sundararajan, *Journal of Electrostatics* 63, 297–307 (2005).
3. U. Hassan, T. Ghonge, B. Reddy Jr., M. Patell, M. Rappleye, I. Taneja, A. Tanna, R. Healey, N. Mansury, Z. Price, T. Jensen, J. Berger, A. Hasnain, E. Flaughner, S. Liu¹, B. Davis, J. Kumar, K. White & R. Bashir (2017) 10.1038/ncomms15949 | www.nature.com/naturecommunications.
4. U. Hassan, B. Reddy, G. Damhorst, O. Sonoiki, T. Ghonge, C. Yang and R. Bashir, *Technology* (2015).
5. HIV.Gov. (2018), <https://www.hiv.gov/hiv-basics/overview/data-and-trends/global-statistics>
6. U.Hassan, N.Watkins, , B. Reddy,G. Damhorst and R. Bashir, *Protocol* (2016)
7. Y. Hou, Controlling Variables of Electric Double-Layer Capacitance, <https://core.ac.uk/download/pdf/61363805.pdf>, Accessed 23 October, 2018.
8. S. Gawad, L. Schildb and Ph. Renauda, *Lab on a Chip*, 2001, 1, 76–82 (2001).
9. M. Khine, A. Lau, C. Ionescu-Zanetti, J. Seo and L. Lee (2004) <https://doi.org/10.1039/b408352k>.
10. Lenntech, Water treatment and purification (2018), <https://www.lenntech.com/applications/ultrapure/conductivity/water-conductivity.htm>
11. K. Schoenbach, S. Katsuki, R. Stark, E. Buescher and S.Beebe, *IEEE Transactions on Plasma Science* (2002).
12. H.Schwan, *Electroporation and Electrofusion in Cell Biology*, 1st edn. (Plenum press, New York, 1998), pp. 3-21
13. E. Valera, J. Berger, U. Hassan, T.Ghonge, J. Liu, M. Rappleye, J. Winter, D. Abboud, Z. Haidry, R. Healey, NT. Hung, N. Leung, N. Mansury, A. Hasnain, C. Lannon, Z. Price, K. White and R. Bashir, *Lab Chip* (2018).
14. J. Vibha, W. Pramod. P, J. Sameer, *International Nanoelectronics Conference* (2013).

16. Q, Xiaolong, H. Jen-Huang, M. Trisha, Microfluidic channel optimization to improve hydrodynamic dissociation of cell aggregates and tissue, *Nature* (2018).
17. N. Watkins, U. Hassan, G. Damhorst, H. Ni, A.Vaid, W. Rodriguez and R. Bashir, *Science Translational Medicine* (2013),[https://doi.org/ 0.1126/scitranslmed.3006870](https://doi.org/0.1126/scitranslmed.3006870)
18. World Health Organization (2018),
<http://www.who.int/hiv/en/>
19. Gawad S, Cheung K, Seger U, Bertsch A and Renaud Ph 2004, Dielectric spectroscopy in a micromachined flow cytometer: theoretical and practical considerations *Lab Chip* 4 241–51
20. Morgan, Hywel, Tao Sun, David Holmes, Shady Gawad, and Nicolas G. Green. "Single cell dielectric spectroscopy." *Journal of Physics D: Applied Physics* 40, no. 1 (2006): 61.
21. Asami, K., 2006. Dielectric dispersion in biological cells of complex geometry simulated by the three-dimensional finite difference method. *Journal of Physics D: Applied Physics*, 39(3), p.492.
22. Schwan H P, Takashima S, Miyamoto V K and Stoeckenius W 1970 Electrical properties of phospholipid vesicles *Biophys. J.* 10 1102–19
23. Sekine K 2000 Application of boundary element method to calculation of the complex permittivity of suspensions of cells in shape of D_{∞h} symmetry *Bioelectrochemistry* 52 1–7
24. Foster K R and Schwan H P 1989 Dielectric properties of tissues and biological materials: A Critical Review *Critical Rev. Biomed. Eng.* 17 25–104
25. Gimsa J and Wachner D 1998 A unified resistor-capacitor model for impedance, dielectrophoresis, electrorotation and induced transmembrane potential *Biophys. J.* 75 1107–16
26. Gowrishankar T R and Weaver J C 2003 An approach to electrical modeling of single and multiple cells *Proc. Natl. Acad. Sci. USA* 100 3203–8
27. Stewart D A Jr, Gowrishankar T R, Smith K C and Weaver J C 2005 Cylindrical cell membranes in uniform applied electric fields: validation of a transport lattice method *IEEE Trans. Biomed. Eng.* 10 1643–53